THE JOURNAL OF PHYSICAL CHEMISTRY B

Article

Crowding Effects on the Mechanical Stability and Unfolding Pathways of Ubiquitin

David L. Pincus, and D. Thirumalai

J. Phys. Chem. B, **2009**, 113 (1), 359-368 • DOI: 10.1021/jp807755b • Publication Date (Web): 10 December 2008

Crowding Effects on the Mechanical Stability and Unfolding Pathways of Ubiquitin

David L. Pincus[†] **and D. Thirumalai***[,†,‡]

Biophysics Program, Institute for Physical Science and Technology, and Department of Chemistry and Biochemistry, University of Maryland, College Park, Maryland 20742

Received: September 1, 2008; Revised Manuscript Received: October 17, 2008

The interiors of cells are crowded, thus making it important to assess the effects of macromolecules on the folding of proteins. Using the self-organized polymer (SOP) model, which is a coarse-grained representation of polypeptide chains, we probe the mechanical stability of ubiquitin (Ub) monomers and trimers ($(Ub)_3$) in the presence of monodisperse spherical crowding agents. Crowding increases the volume fraction (Φ_c)-dependent average force ($\langle f_u(\Phi_c)\rangle$), relative to the value at $\Phi_c = 0$, needed to unfold Ub and the polyprotein. For a given Φ_c, the values of $\langle f_u(\Phi_c)\rangle$ increase as the diameter (σ_c) of the crowding particles decreases. The average unfolding force $\langle f_u(\Phi_c)\rangle$ depends on the ratio D/R_g, where $D \approx \sigma_c(\pi/6\Phi_c)^{1/3}$, with R_g being the radius of gyration of Ub (or $(Ub)_3$) in the unfolded state. Examination of the unfolding pathways shows that, relative to $\Phi_c = 0$, crowding promotes reassociation of ruptured secondary structural elements. Both the nature of the unfolding pathways and $\langle f_u(\Phi_c)\rangle$ for $(Ub)_3$ are altered in the presence of crowding particles, with the effect being most dramatic for the subunit that unfolds last. We predict, based on SOP simulations and theoretical arguments, that $\langle f_u(\Phi_c)\rangle \sim \Phi_c^{1/3\nu}$, where ν is the Flory exponent that describes the unfolded (random coil) state of the protein.

Introduction

Cells exist in a crowded environment consisting of macromolecules (lipids, mRNA, ribosome, sugars, etc.), making it critical to investigate protein folding in the presence of crowding agents.[1] If the interactions between the crowding agents and the protein of interest are short-ranged and nonspecific (as is often the case), then the volume excluded by the crowding agents prevents the polypeptide from sampling extended conformations. As a consequence, the entropy of the denatured state ensemble (DSE) decreases relative to the case when the crowding agents are absent. These arguments suggest that excluded volume of crowding agents should enhance the stability of the folded state, provided that the crowding-induced changes in the native state are negligible.[2,3] The entropic stabilization mechanism, described above, has been used in several theoretical models to quantitatively describe the extent of the folded protein as a function of the volume fraction, Φ_c, of the crowding agents.[3,4] More recently, a theory whose origins can be traced to the concept of intraprotein attraction due to depletion of crowding agents near the protein[5−7] predicts that the enhancement in stability is $\Delta T(\Phi_c) = T_f(\Phi_c) - T_f(\Phi_c = 0) \sim \Phi_c^{\alpha}$, where $T_f(\Phi_c)$ is the folding temperature at Φ_c and α is related to the Flory exponent that characterizes the size of the protein in the DSE.[3] From this prediction, it follows that crowding affects the DSE to a greater extent than that in the folded state. Although the precise theoretical predictions of the power law change in $\Delta T(\Phi_c)$ as Φ_c changes have not been verified, several experiments using a number of proteins have confirmed that indeed $T_f(\Phi_c)$ increases with Φ_c.[8−10] It cannot be emphasized enough that the theory described here applies only to cases when the crowding interactions between crowding agents and proteins and between crowding particles themselves are purely repulsive.

While much less is known about the effects of crowding on the folding kinetics, Cheung et al.[3] predicted that the entropic stabilization also suggests that the folding rates should increase at moderate values of Φ_c. They suggest that crowding can enhance folding rates by a factor of $e^{-\Delta S(\Phi_c)/k_B}$, where $\Delta S(\Phi_c)$ ($\sim\Phi_c^{\alpha}$) is the decrease in the entropy of the DSE relative to its value in the bulk. From the arguments of Cheung et al.,[3] it follows that the equilibrium changes in the entropy ($\Delta S(\Phi_c)$) of the DSE, with respect to the bulk, should also determine rate enhancement provided that neither the barriers to folding[11] nor the native state is perturbed significantly by crowding particles.

Single-molecule force spectroscopy, such as atomic force microscopy (AFM) and laser optical tweezers, have been used to monitor the behavior of biopolymers under tension and are ideally suited to probe the enhancement in crowding-induced stability by a direct measure of $f_u(\Phi_c)$. Indeed, Ping et al.[12] have recently investigated the effect of dextran molecules on the mechanical stability of $(Ub)_8$. The eight Ub (Figure 1A) modules were N−C linked (i.e., modules i and i + 1 were chemically linked together in a head-to-tail manner). They found that the average force required to unfold a module, $\langle f_u(\Phi_c)\rangle$, increased by 21% as the dextran concentration, ρ, was increased from 0 to 300 g/L at $r_f = 4.2 \times 10^3$ pN/s. Similar results have been obtained recently by Yuan et al. at $r_f = 12.5 \times 10^3$ pN/s.[13]

Motivated in part by experiments,[12,13] we used simulations to investigate the effects of crowding agents on the mechanical stability of a protein subject to external tension. We focused on ubiquitin (Ub), a 76 residue protein composed of 5 β strands and 2 α helices (Figure 1A), and confined our investigation to nonequilibrium "force-ramp" experiments.[14] The primary data recorded during such an experiment is a trace of the force exerted on the tip as a function of the extension of the molecule, a force-extension curve (FEC). When the force exceeds some critical value, the FEC displays a sudden increase in length and is often accompanied by a concomitant sharp decrease in force.

* To whom correspondence should be addressed. Phone: 301-405-4803. Fax: 301-314-9404. E-mail: thirum@umd.edu.
† Institute for Physical Science and Technology.
‡ Department of Chemistry and Biochemistry.

10.1021/jp807755b CCC: $40.75
Published on Web 12/10/2008

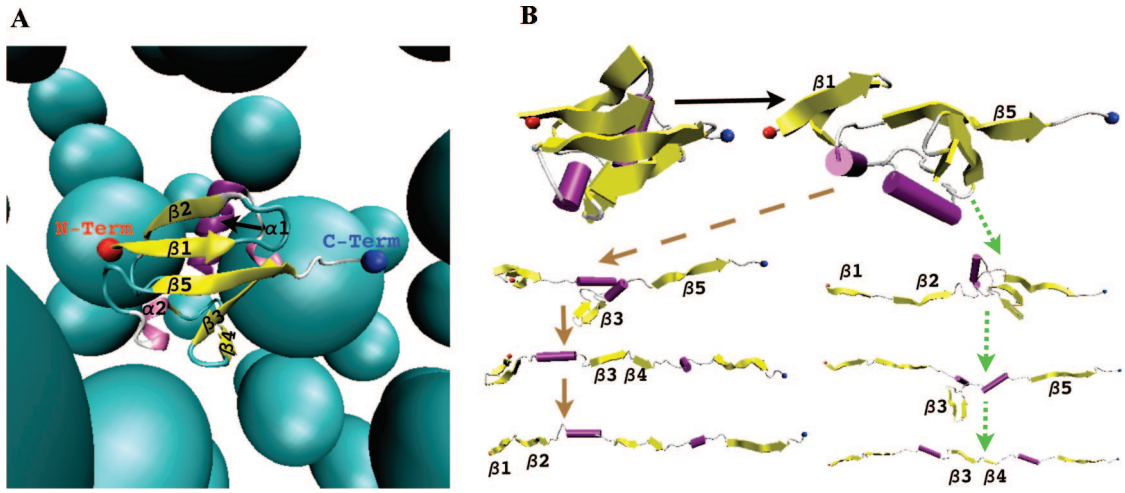

Figure 1. (A) Cartoon representation of the native structure of ubiquitin (PDB accession id 1UBQ) in the presence of spherical crowding agents. The five beta strands, labeled $\beta1$ through $\beta5$, are colored in yellow. The two alpha helices ($\alpha1$ and $\alpha2$) are shown in purple. The N- and C-terminal beads are represented as spheres. In our simulations the N-terminal bead was held fixed while the C-terminal bead was pulled via a tethered spring. (B) Snapshots from an unfolding trajectory illustrating the main ubiquitin (Ub) unfolding pathway (brown dashed arrows) and an alternate unfolding pathway (green dotted arrow). In both pathways, the initial unfolding event corresponds to separation of the C-terminal strand $\beta5$ from the N-terminal strand $\beta1$. Along the main pathway, this is quickly followed by separation of $\beta5$ from $\beta3$. The penultimate rupture event along the main pathway corresponds to disruption of the $\beta3/\beta4$ strand pair, while the N-terminal $\beta1/\beta2$ strand pair is the last to break. The trajectory illustrated here was generated at $\Phi_c = 0.0$ and $r_f = 160 \times 10^3$ pN/s. An alternate pathway was observed at $\Phi_c = 0.0$ and $r_f = 4 \times 10^3$ pN/s. Along this pathway, separation of $\beta5$ from $\beta1$ is followed by separation of $\beta1/\beta2$. The final two rupture events correspond to those of the $\beta5/\beta3$ contacts and $\beta3/\beta4$ strand pair, respectively. (Figures generated with VMD.[43])

Presumably, the sharp change corresponds to the unfolding of the protein. Typical AFM experiments use tandem arrays of proteins which are chemically linked together (often through genetic engineering). We use the term module to denote a protein of the array. The FEC resulting from such an experiment reveals several equally spaced peaks punctuated by sharp increases in the extension of the molecule corresponding to the unfolding of individual modules. The height of these force peaks and their shape depend on the loading rate, $r_f = k_s \times v$, where k_s is the cantilever's spring constant and v is the (constant) speed at which the stage is retracted away from the cantilever.[15]

In order to compare to experiments, our simulations are performed using coarse-grained models for which simulations can be done at r_f that are comparable to those in AFM experiments. Our work has led to a number of testable results. (1) At $\Phi_c = 0.3$, the average unfolding force for Ub increases by at most only 7% compared to that at $\Phi_c = 0$. We find that $\langle f_u(\Phi_c)\rangle$ in small crowding agents is greater than that in larger particles. (2) In the presence of crowding agents, secondary structural elements re-form multiple times even after initial rupture. (3) Although large crowding particles are predicted to have a smaller effect on $\langle f_u(\Phi_c)\rangle$ (for a given Φ_c), they can profoundly affect the unfolding of polyUb. We predict that $\langle f_u(\Phi_c)\rangle$ for a given subunit depends on the number of already unfolded portions of the polyprotein. This result is important because many naturally occurring proteins that are subject to tensile stresses exist as tandem arrays of modules. It further suggests that the existence of such redundancy can more properly be understood in the context of a crowded cellular milieu.

Methods Sections

Self-Organized Polymer Model for Ub. We used a coarse-grained model for proteins to investigate crowding effects on the mechanical stability of Ub and $(Ub)_3$ at loading rates that are comparable to those used in AFM experiments.[12,13] We assumed that Ub could be described using the self-organized polymer (SOP) model, a model that has been successfully used to make a number of predictions regarding the unfolding of proteins and RNA,[16,17] allosteric transitions in enzymes,[18,19] and movement of molecular motors on polar tracks.[20] Previous studies[21] have used more standard Go models[22,23] to probe various aspects of forced unfolding of Ub. The SOP energy function (E_p) for a protein with N amino acids, specified in terms of the C_α coordinates r_i ($i = 1, 2, \ldots, N$), is

$$E_p = E_{FENE} + E_{nb}^{att} + E_{nb}^{rep} = -\sum_{i=1}^{N-1} \frac{k}{2} R_0^2 \ln\left[1 - \frac{(r_{i,i+1} - r_{i,i+1}^0)^2}{R_0^2}\right] + \sum_{i=1}^{N-3}\sum_{j=i+3}^{N} \varepsilon_h\left[\left(\frac{r_{ij}^0}{r_{ij}}\right)^{12} - 2\left(\frac{r_{ij}^0}{r_{ij}}\right)^{6}\right]\Delta_{ij} + \sum_{i=1}^{N-2}\sum_{j=i+2}^{N} \varepsilon_l\left(\frac{\sigma}{r_{ij}}\right)^6 (1 - \Delta_{ij}) \quad (1)$$

where $r_{ij} = |\mathbf{r}_i - \mathbf{r}_j|$, $r_{ij}^0 = |\mathbf{r}_i^0 - \mathbf{r}_j^0|$ is the value of r_{ij} in the native structure, $k = 2 \times 10^3$ kcal/(mol·nm^2), $\varepsilon_h = 1.4$ kcal/mol, $\varepsilon_l = 1.0$ kcal/mol, and $\sigma = 0.38$ nm. Note that $k_BT \approx 0.6$ kcal/mol ≈ 4.2 pN·nm. In eq 1, $\Delta_{ij} = 1$ if $r_{ij}^0 < 0.8$ nm and $\Delta_{ij} = 0$ otherwise. Native coordinates corresponded to those of the C_α atoms of the 1.8 Å resolution Protein Data Bank crystal structure 1UBQ.[24] For Ub, $N = 76$ and 228 for $(Ub)_3$. The first term in eq 1 is the FENE potential[25] that accounted for chain connectivity. The second (Lennard-Jones) term accounted for the nonbonded interactions that stabilize the native state, and the final (soft-sphere) term accounted for excluded-volume interactions (including those of an angular nature). The SOP model is different from the Go model because there are no angular terms in SOP, and the connectivity is enforced differently as well. The SOP representation of the polypeptide chain is in the same spirit as other coarse-grained models used in polymers.[26]

Crowding Particles and Interactions with Ub. We assumed that the crowding particles are spherical with diameter σ_c (σ_c = 6.4 nm in some simulations, while σ_c = 1.0 nm in others). Crowders interacted among themselves and with the protein, respectively, via the following LJ potentials

$$E_{cc} = 4\varepsilon_l\left(\left(\frac{\sigma_{cc}}{r}\right)^{12} - \left(\frac{\sigma_{cc}}{r}\right)^{6} + \frac{1}{4}\right)\Theta(r_{min}^{cc} - r) \quad (2)$$

$$E_{cp} = 4\varepsilon_l\left(\left(\frac{\sigma_{cp}}{r}\right)^{12} - \left(\frac{\sigma_{cp}}{r}\right)^{6} + \frac{1}{4}\right)\Theta(r_{min}^{cp} - r) \quad (3)$$

where $\sigma_{\alpha\beta} = (\sigma_\alpha + \sigma_\beta)/2$, $\sigma_p = \sigma = 0.38$ nm, $r_{min}^{cc} = 2^{1/6}\sigma_{cc}$, and $r_{min}^{cp} = 2^{1/6}\sigma_{cp}$. The Heaviside functions truncate the potentials at their minima and thereby ensure that only the repulsive portions of eq 2 and 3 contribute to interactions involving crowding agent.

Mimics of Crowding Using Asakura−Oosawa Theory. Even using a coarse-grained SOP representation of proteins, it is difficult to carry out converged simulations in the presence of crowding agents. The reason is that the number of crowding agents can be large. Moreover, the separation in the spatial and temporal scales of the protein and the crowding particles has to be carefully considered to obtain reliable results. In light of these difficulties, it is of interest to consider the effective attraction between the sites on the protein using the implicit pairwise potential computed by Asakura and Oosawa. The intramolecular attraction arises due to the depletion of crowding particles near the protein. To probe the efficacy of these models, we employed in some simulations the Asakura−Oosawa model[5−7] of crowding effects. For these simulations, we added the following term to the bare SOP Hamiltonian (eq 1)

$$E_{AO}(r_{ij}) = -\Phi_c k_B T \sum_{j\geq i+3}\left(\frac{(\sigma+\sigma_c)}{\sigma_c}\right)^3 \times \left(1 - \frac{3r_{ij}}{2(\sigma+\sigma_c)} + \frac{r_{ij}^3}{2(\sigma+\sigma_c)^3}\right)\sigma < r_{ij} < \sigma + \sigma_c \quad (4)$$

where σ = 0.38 nm, σ_c = 6.4 nm, Φ_c = 0.3, $k_BT \simeq 4.2$ pN·nm, and r_{ij} is the distance separating protein beads i and j.

$(Ub)_3$ Intermodule Interactions. For simulations involving $(Ub)_3$, residues in different modules interacted via

$$E_{pp} = \varepsilon_l\left(\frac{\sigma}{r}\right)^6 \quad (5)$$

where r is the distance separating the two beads. Note that this potential is short-ranged and purely repulsive and that it is the same potential used for non-native intraprotein interactions.[17]

Simulation Details. $\Phi_c = 0$. Hundreds of simulations of 5 × 10^6 steps (≃30 μs) at T = 300 K were used to generate initial structures for use in the pulling simulations. The protein was completely free in solution (i.e., no forces were applied to either terminus), and no crowders were present during the equilibrations. The N-terminus of the protein was subsequently translated to the origin, and the protein was rotated such that its end-to-end vector, **R**, (i.e., the vector pointing from the N-terminal bead to the C-terminal bead) coincided with the pulling ($+z$) direction.

An unfolding trajectory was initiated by selecting a random initial structure from among the set of thermally equilibrated structures and by tethering a harmonic spring to the C-terminal bead. The N-terminal bead was held fixed throughout the simulations. Tension was applied to the protein by displacing the spring along the $+z$ axis and resulted in application of the following force to the C-terminal bead

$$f_z = -k_s([z(t) - z(0)] - [z_s(t) - z_s(0)]) \quad (6)$$

where k_s is the spring constant, $z(t) = \mathbf{R}(t)\cdot\hat{z}$, and $z_s(t)$ corresponds to the displacement of the end of the spring. Note that k_s was also used to constrain the simulation to the z-axis; $f_x = -k_s[x(t) - x(0)]$ and $f_y = -k_s[y(t) - y(0)]$. The displacement of the spring was updated at every time step.

We simulated forced unfolding of monomeric Ub at four different r_f values (160 × 10^3, 80 × 10^3, 20 × 10^3, and 4 × 10^3 pN/s), while simulations on N−C-linked $(Ub)_3$ were performed at $r_f = 640 \times 10^4$ pN/s. All overdamped force-ramp simulations were performed at the same speed, υ = 10312 nm/s, and spring constants were varied over a range from 0.3879 to 31.032 pN/nm to achieve the aforementioned r_f (via the relation $r_f = k_s\upsilon$). Our simulations were realistic because they maintained loading rates consistent with experiment and because r_f is the prime determinant of the unfolding pathway.[15]

$\Phi_c \neq 0.0$. Simulations involving explicit crowders were carried out at a fixed volume fraction of Φ_c = 0.3 and with a fixed number N_c = 100 of crowding spheres. (N_c was fixed to render the problem computationally tractable.) By using the relation $\Phi_c = (N_c\pi/6)(\sigma_c/L)^3$, we adjusted the length of a side of the cubic simulation box (L) to maintain Φ_c = 0.3. Thus, L = 35.8 nm when σ_c = 6.4 nm and L = 5.6 nm when σ_c = 1.0 nm. Explicit crowders were added to the simulation after loading an equilibrated structure but before the application of tension. Initial crowder positions were chosen randomly and in a serial manner from a uniform distribution. If the distance between an initial crowder position and that of another crowder or protein bead did not exceed the sum of their radii, then the prospective position was rejected and another random position chosen to avoid highly unfavorable steric overlaps.

Periodic boundary conditions (PBC) and the minimum image convention[27] were employed in the simulations. Two sets of coordinates were stored for protein beads at every time step; PBC were applied to one set, and the other was propagated without PBC. Distances between protein beads were calculated from the uncorrected set of coordinates without minimum imaging, while protein−crowder distances were calculated from the PBC coordinates with minimum imaging.

To improve simulation efficiency, a cell list[27] was used to calculate crowder−crowder and protein−crowder interactions. The entire simulation volume was partitioned into 64 subvolumes, and it was only necessary to calculate interactions within a subvolume and between beads of the subvolume and those of 13 of its 26 neighbors. The cell list was updated at every time step to ensure the accuracy of the simulations.

The equations of motion in our overdamped simulations (used in all force-ramp simulations) were integrated with a time step of $h = 0.01\tau_L$ (τ_L = 2.78 ps) using the method of Ermak and McCammon.[28] The friction coefficient of the crowders, ζ_c, was determined via the relation $\zeta_c/\zeta = \sigma_c/\sigma$, where σ_c is the crowder diameter, σ = 0.38 nm is the diameter of a protein bead, and $\zeta = 83.3 \times (m/\tau_L) = 9 \times 10^{-9}$ g/s is the friction coefficient associated with a protein bead of mass $m = 3 \times 10^{-22}$ g. Simulated times were translated into real times using $\tau_H = (\zeta\varepsilon_h/$

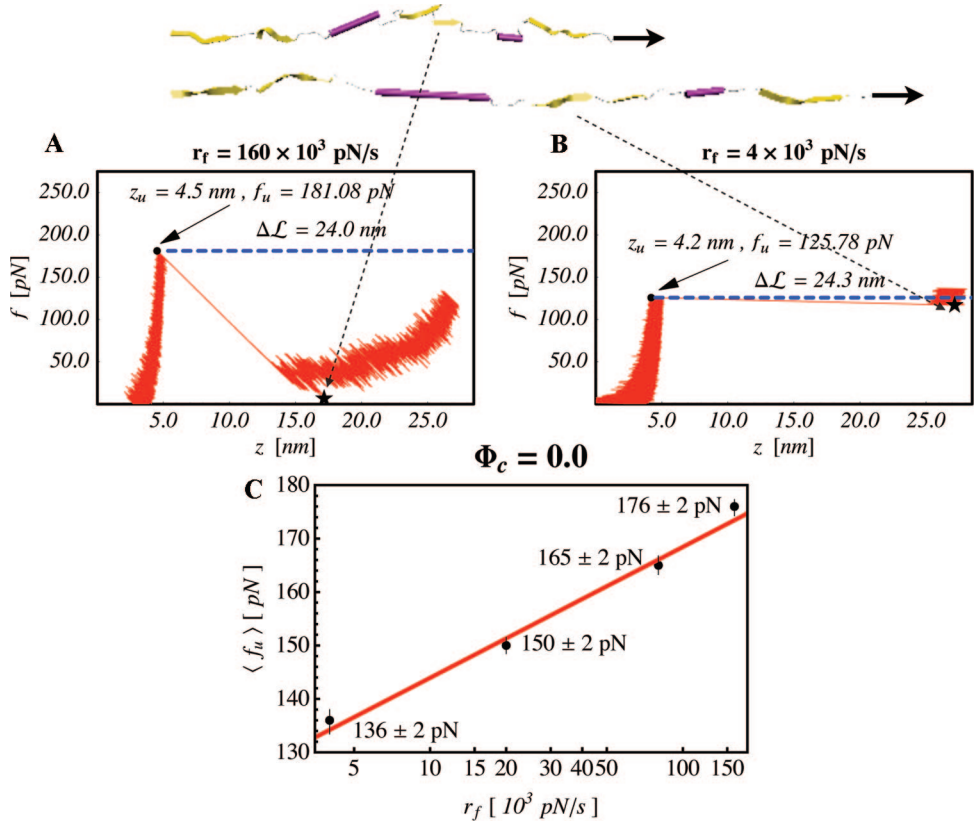

Figure 2. Force-extension curves (FECs) at two different loading rates, (A) $r_f = 160 \times 10^3$ pN/s and (B) $r_f = 4 \times 10^3$ pN/s. Data from the simulation is presented as a red trace. For each trajectory, a black arrow points to the unfolding force, f_u. The z_u corresponds to the extension of the molecule along the pulling (i.e., z) direction evaluated at f_u. $\Delta\mathcal{L}$ (dotted blue line) is the contour length increment and is a measure of the amount of chain released in an unfolding event. We measured $\Delta\mathcal{L}$ as $\mathcal{L} - z_u$, where $\mathcal{L} = (N - 1) \times \sigma = 75 \times 0.38$ nm is a nominal contour length of 28.5 nm. Stars in each subfigure mark the minimum force observed after an unfolding event, and chain conformations corresponding to the starred points in figures A and B are illustrated at the top of the figure. Unfolding events at smaller r_f resulted in larger molecular extensions before significant resistance was encountered. (Yellow arrows correspond to β strands and purple cylinders correspond to α helices.) (The figures were generated with VMD.[43]) (C) $\langle f_u \rangle$ versus r_f evaluated at $\Phi_c = 0$. The red curve corresponds to a linear least-squares fit to the set of basis functions $\{1, \ln(r_f)\}$ and demonstrates that $\langle f_u \rangle \sim \ln(r_f)$. (Note that the abscissa is a log scale.) Each point is labeled as mean ± standard error. Statistics at $r_f = 160 \times 10^3$, 80×10^3, 20×10^3, and 4×10^3 pN/s were calculated from 50, 49, 50, and 16 trajectories respectively.

$k_BT) \times \tau_L \times (\tau_L/m)$.[29] At $T = 300$ K, $\tau_H = 543.06$ ps, and since $h = 0.01 \times \tau_L$, the real time per step is 5.4306 ps.

Results and Discussion

Monomeric Ub at $\Phi_c = 0.0$. At $\Phi_c = 0.0$, forced unfolding of Ub was simulated at four different r_f values (4×10^3, 20×10^3, 80×10^3, 160×10^3 pN/s), where the lowest value corresponds approximately to the value used in the pulling experiments of Ping et al.,[12] and all r_f's are experimentally accessible.

Force Profiles. Figure 2A and B provides examples of FECs collected at the highest and lowest r_f's. We used a nominal contour length of $(N - 1)\sigma = 75 \times 0.38$ nm and unfolding forces, f_u, to determine contour length increments, $\Delta\mathcal{L}$, for each trajectory at $r_f = 160 \times 10^3$ pN/s (Figure 2A). We identified f_u with the peak of the FEC before the stick−slip transition.[30,31] The average extension $\langle \Delta\mathcal{L} \rangle = 23.991 \pm 0.010$ nm is in excellent agreement with the experimental result of 24 ± 5 nm found by Carrion-Vazquez et al.[30] The projection (z_u) of the end-to-end vector at f_u in the z-direction varied between 4.1 and 4.7 nm, depending on r_f. Since the native end-to-end distance is $z_0 = 3.7$ nm, $z_u - z_0 \equiv \Delta z_u$ ranges from 0.4 to 1.0 nm. The lower end of this range is slightly larger than the 0.25 nm transition-state distance for the mechanical unfolding of the structurally similar titin immunoglobulin domains.[32] Indeed, we expect $\Delta z_u > 0.25$ nm because of the nonequilibrium nature of the simulations. Larger r_f values typically lead to larger $\langle \Delta z_u \rangle$ ($\sim [k_BT/\langle f_u \rangle] \ln(r_f)$).

Average unfolding forces, $\langle f_u(\Phi_c) \rangle$, depended approximately logarithmically on r_f[15] (Figure 2C), and $\langle f_u(r_f = 4 \times 10^3 \text{ pN/s}) \rangle = 136$ pN is in fair agreement with the experimental value of 166 ± 33 pN observed by Ping et al.[12] at $r_f = 4.2 \times 10^3$ pN/s. The $\langle z_u \rangle$ also showed a logarithmic dependence on r_f, but the difference between the value calculated at $r_f = 160 \times 10^3$ pN/s and that calculated at $r_f = 4 \times 10^3$ pN/s is small (≃2 Å). Although the underlying free-energy landscape is time-dependent in a nonequilibrium force-ramp pulling experiment, these results suggest that the distance from the native state to the transition state is small. It is likely that at loading rates that are achieved in laser optical tweezer experiments (~10 pN/s), the location to the transition state would increase because of the response of biopolymers to loading rate changes from being plastic (low r_f) to brittle (high r_f).[33]

Unfolding Pathways. In the dominant pathway, unfolding proceeded in a fairly Markovian fashion with the primary order of events following the sequence $\beta1/\beta5 \rightarrow \beta3/\beta5 \rightarrow \beta3/\beta4 \rightarrow \beta1/\beta2$ (Figures 1B and 3). This is precisely the same sequence as that seen in the simulations by Li et al.[23] Alternative pathways, reminiscent of kinetic partitioning[34] observed in the forced unfolding of GFP[35] and lysozyme,[36] were also infrequently sampled. For example, at $r_f = 4 \times 10^3$ pN/s, ~6% of the trajectories unfolded as follows, $\beta1/\beta5 \rightarrow \beta1/\beta2 \rightarrow \beta3/\beta5$

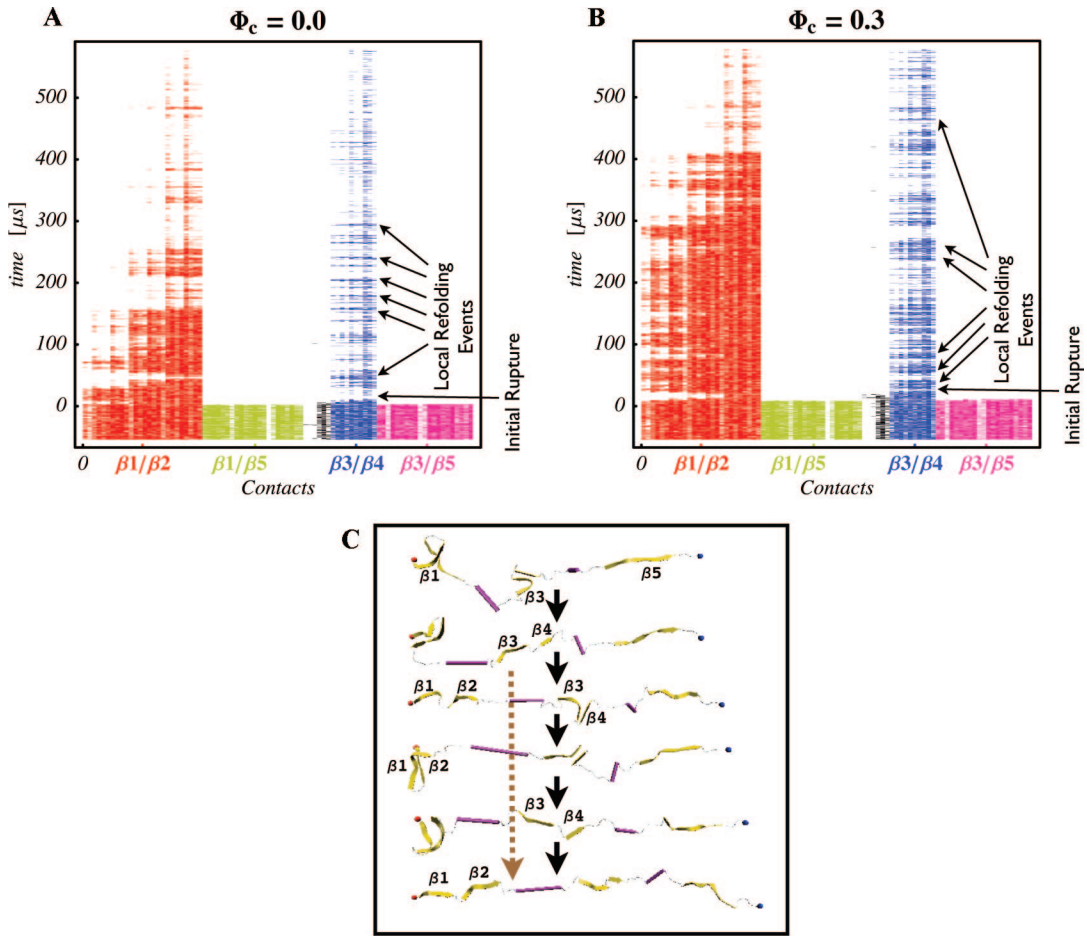

Figure 3. Rupture events at $\Phi_c = 0.0$ (***A***) and at $\Phi_c = 0.3$ and $\sigma_c = 6.4$ nm (***B***). The figure illustrates that after the initial rupture event at step 0, subsequent unfolding was affected by the crowding agent. $\beta1/\beta2$ contacts and $\beta3/\beta4$ persisted longer, and there were many more local refolding events in the presence of the crowders (B) than in their absence (A). (C) Snapshots from an unfolding trajectory at $\Phi_c = 0.3$ and $r_f = 4 \times 10^3$ pN/s illustrate the primary difference between unfolding at $\Phi_c = 0.3$ and that at $\Phi_c = 0.0$. The brown dotted arrow shows unfolding without any local refolding events, while the sequence of black arrows illustrates local rupture and refolding events. The hallmark of forced unfolding in a crowded environment is repeated breaking and re-forming of contacts after an initial rupture event. (The figures were generated with VMD.[43])

$\rightarrow \beta3/\beta4$ (Figure 1B), while the remaining ~94% followed the dominant pathway. At the highest loading rate, one frequently observed the following sequence of events, $\beta1/\beta5 \rightarrow \beta3/\beta5 \rightarrow \beta1/\beta2 \rightarrow \beta1/\beta2$ (reform) $\rightarrow \beta3/\beta4 \rightarrow \beta1/\beta2$, where $\beta1/\beta2$ ruptured but then re-formed prior to the rupture of $\beta3/\beta4$. As illustrated in Figure 2A and B, unfolding events at smaller r_f tended to result in larger molecular extensions.

The nonequilibrium character of a pulling experiment decreased with decreasing r_f, and smaller r_f resulted in smaller force drops after the unfolding force, f_u, is reached. Since the force applied by the spring to the end of the protein did not fall off as sharply at lower r_f, more of the protein was extended during an unfolding event. The smaller extensions following unfolding events at higher r_f (relative to those observed at lower r_f) were responsible for the $\beta1/\beta2$ unfolding/refolding events mentioned above because the applied tension was very low after the initial rupture event (Figure 2A and B). At lower r_f, this situation no longer held because the initial unfolding event resulted in a chain extension that was a significant fraction of the chain's contour length (Figure 2B).

Crowding Effects on Ub ($\Phi_c = 0.3$). Depletion forces stabilize proteins and shift the folding equilibrium toward more compact states.[37] These forces result from an increase in the entropy of the crowding agents that more than compensates for an increase in the free energy of a protein molecule upon compaction. Simulations of forced unfolding of Ub in the presence of explicit crowders of diameters $\sigma_c = 6.4$ and 1.0 nm were used to assess the contribution of the depletion forces to mechanical stability. Sixteen trajectories were collected for each r_f investigated. Three r_f's (20×10^3, 80×10^3, and 160×10^3 pN/s) were explored for the $\sigma_c = 6.4$ nm sized depletants. Only the two highest r_f values (80×10^3 and 160×10^3 pN/s) were explored for the $\sigma_c = 1.0$ nm sized crowders.

Small Crowding Particles Increase Unfolding Forces. Example FECs collected in the presence of crowders of diameter $\sigma_c = 6.4$ and 1.0 nm are illustrated in Figure 4A and B. The $\sigma_c = 6.4$ nm curves in Figure 4 look qualitatively very similar to those seen at $\Phi_c = 0.0$, while the FECs collected at $\sigma_c = 1.0$ nm look qualitatively different. For example, larger $\langle f_u \rangle$ than those observed at either $\Phi_c = 0.0$ or in the presence of the $\sigma_c = 6.4$ nm crowders are apparent in the FECs collected at $\sigma_c = 1.0$ nm (Figure 4A and B). Indeed, Figure 4C reveals that this observation is quantitatively accurate. Although the $\langle f_u \rangle$ in the presence of the $\sigma_c = 6.4$ nm crowders was statistically indistinguishable from the $\langle f_u \rangle$ at $\Phi_c = 0$ (compare Figure 4C with Figure 2C), the average unfolding forces in the presence of the $\sigma_c = 1.0$ nm crowders were statistically greater than those measured at $\Phi_c = 0.0$. At $r_f = 160 \times 10^3$ pN/s, the $\langle f_u(\Phi_c = 0.3) \rangle$ in the presence of the $\sigma_c = 1.0$ nm crowders exceeded that at $\Phi_c = 0.0$ by 3%, while at $r_f = 80 \times 10^3$ pN/s, the increase was 4% (compare Figure 4C with Figure 2C). In one respect, these results are not surprising; it follows from the AO theory

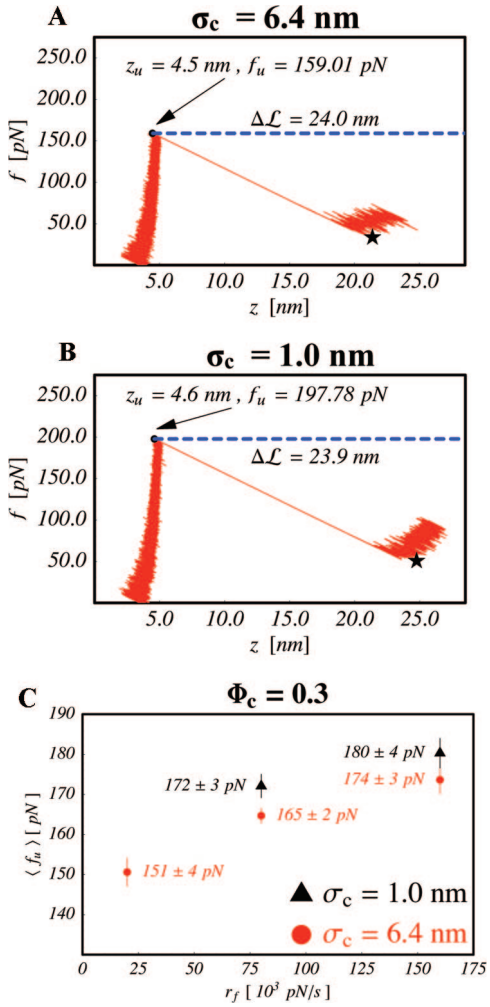

Figure 4. (A) Examples of force extension traces resulting from simulation in the presence of spherical crowding agents of diameter σ_c = 6.4 nm and obtained at $r_f = 80 \times 10^3$ pN/s. (B) Examples of force extension traces resulting from simulation in the presence of spherical crowding agents of diameter σ_c = 1.0 nm and obtained at $r_f = 80 \times 10^3$ pN/s. Both subfigures are labeled as in Figure 2A and B. (C) $\langle f_u \rangle$ versus r_f evaluated at Φ_c = 0.3. Black triangles and red circles correspond to spherical crowders of diameters σ_c = 1.0 and 6.4 nm, respectively. Each point is labeled mean ± standard error. Statistics for each point were calculated from 16 independent trajectories. Only the σ_c = 1.0 nm had an appreciable effect on $\langle f_u \rangle$ when compared to those obtained at identical r_f and at Φ_c = 0.0 (see Figure 2C).

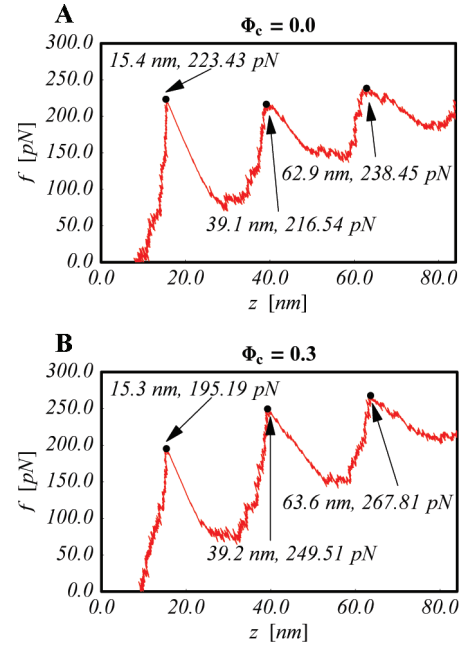

Figure 5. FECs for $(Ub)_3$-forced unfolding at Φ_c = 0.0 (A) and at Φ_c = 0.3 (B). Trajectories were generated at $r_f = 640 \times 10^4$ pN/s and with crowders of diameter σ_c = 6.4 nm. Black arrows mark each trajectory's three unfolding events.

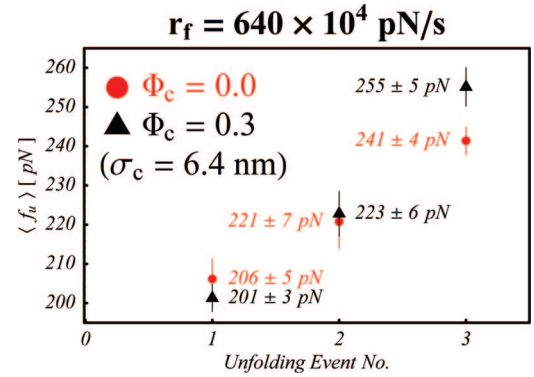

Figure 6. $\langle f_u \rangle$ versus unfolding event number for the unfolding of $(Ub)_3$ in the presence of spherical crowders of diameter σ_c = 6.4 nm (Φ_c = 0.3, black triangles) and in their absence (Φ_c = 0.0, red circles). The individual modules of the polyUb tandem were N−C-linked, and the loading rate was 640×10^4 pN/s. Each point is labeled mean ± standard error. Statistics for each point were calculated from 16 independent unfolding trajectories. An unfolding event corresponded to the unfolding of an individual module. Note that although the crowders had little effect on $\langle f_u \rangle$ for the first and second unfolding events, they had a substantial effect on the last unfolding event. $\langle f_u \rangle$ increased by ≈14 pN for the last unfolding event.

and eq 8 that smaller crowders stabilize Ub more than larger ones. On the other hand, the extent of stabilization (as measured by increases in $\langle f_u \rangle$) was small. We should emphasize that although the increase in the unfolding force is small, the stability change upon crowding is significant. The enhancement in stability is $\Delta G \sim \langle f_u(\Phi_c) \rangle \langle z_{DSE} \rangle \sim 5 k_B T$ using a 3% increase in the unfolding force, and $\langle z_{DSE} \rangle$ is the location of the unfolded basin at ≈5 nm.

Crowding Leads to Transient Local Refolding. The unfolding pathways in the presence of crowding agents of both sizes were very similar to those seen at Φ_c = 0.0. Nevertheless, at Φ_c = 0.3, there tended to be more unfolding/refolding events as the molecule extended past z_u (Figure 3) than that at Φ_c = 0.0. As illustrated, strand pairing between β1 and β2 and between β3 and β4 persisted to a greater extent after the initial unfolding event at Φ_c = 0.3 than that at Φ_c = 0.0. As Ub passed through the point (z_u, f_u), its termini were extended to distances greater than the diameter of even the larger crowders. Depletion forces resulting from the presence of 6.4 nm crowders act on these larger length scales. Assuming that the tension applied to the C-terminus is small enough (e.g., after rupture events at higher loading rates), then such depletion forces can promote re-formation of contacts between secondary structural elements several times during the course of a trajectory. If this is indeed the case, then it suggests that unfolding polyUb may be different from the unfolding of monomeric Ub because depletion effects should increase with the number of modules in the tandem (see below).

AO Model For Forced Unfolding in the Presence of Crowders. We used the Asakura−Oosawa AO model[5−7] (eq 4) of the depletion interaction to model the effects of a crowded environment on Ub. The AO theory has been successfully used to model the effects of a crowded environment on polymers

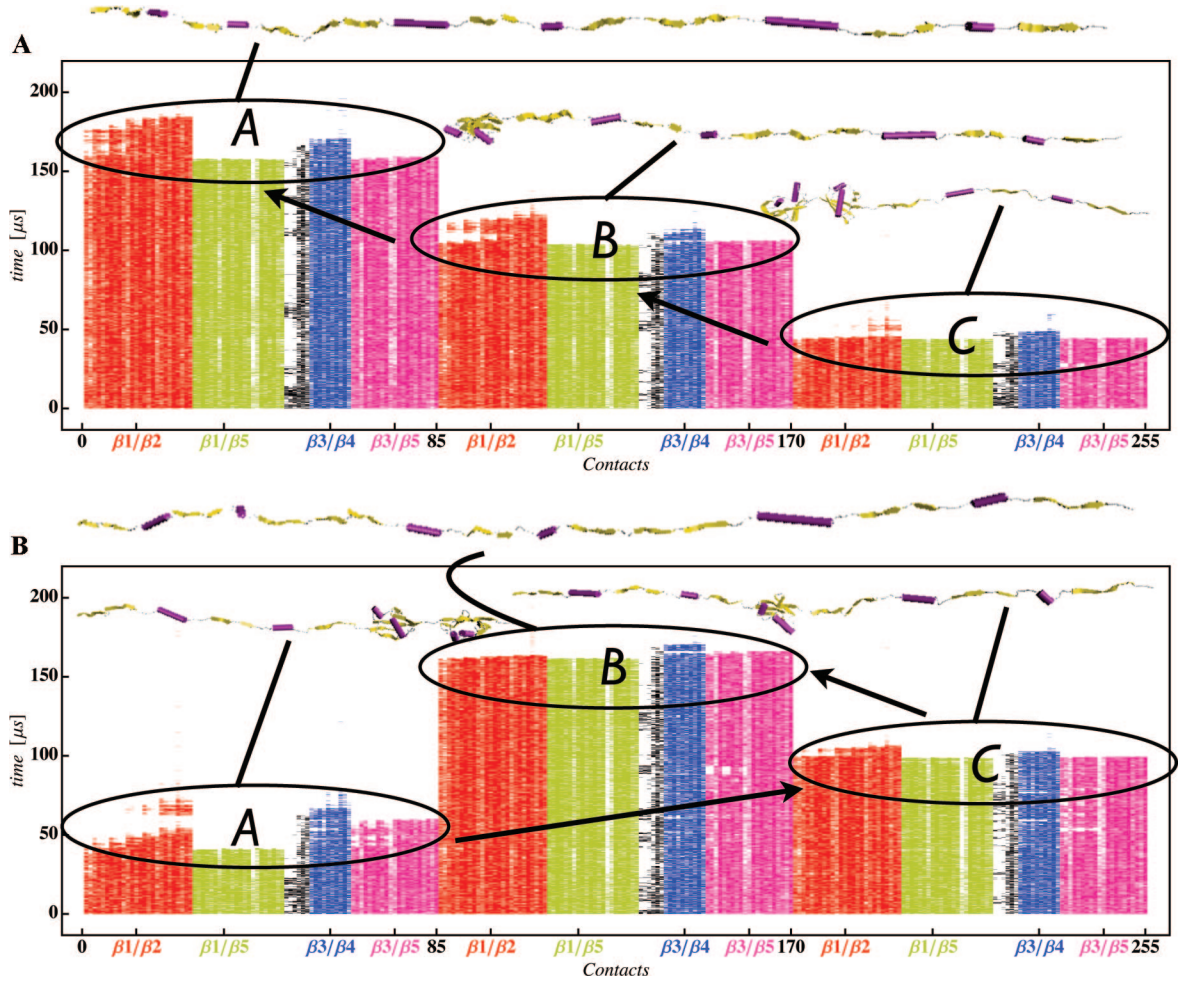

Figure 7. Illustration of the stochastic nature of module unfolding. In (A), module C (the most proximal to the applied force) unfolds first, followed by module B, and finally by rupture of module A. In (B), the order of module unfolding events is A → C → B. The two trajectories illustrated here were both collected at $\Phi_c = 0$ and $r_f = 640 \times 10^4$ pN/s. Table 1 provides the frequencies at which the different possible orders were observed at $\Phi_c = 0$ and at 0.3. The diameter of the crowders is $\sigma_c = 6.4$ nm.

TABLE 1: Module Unfolding Order Frequencies at $\Phi_c = 0$ and 0.3

unfolding order	frequency observed at $\Phi_c = 0$	frequency observed at $\Phi_c = 0.3$
C → B → A	0.44	0.56
C → A → B	0.38	0.13
B → A → C	0.00	0.00
B → C → A	0.13	0.25
A → B → C	0.00	0.00
A → C → B	0.06	0.06

and colloids,[6,7,38,39] and we found that it gives qualitatively accurate results for Ub. We used eq 4 to approximate the effective interaction between spherical protein beads immersed in a crowded solution of volume fraction $\Phi_c = 0.3$. From the form of the AO potential between protein beads, it follows that the range of the potential is proportional to σ_c, but the strength is greater for smaller crowders. Indeed, as revealed in the previous section, simulations in the presence of explicit crowders showed that 1.0 nm crowders resulted in larger average unfolding forces than 6.0 nm crowders (Figure 4C).

Although the AO potential yields qualitatively accurate results, use of the AO potential of eq 4 to implicitly model nonbonded interactions in Ub did not yield quantitatively accurate results. At $r_f = 160 \times 10^3$ pN/s, $\langle f_u(\Phi_c = 0.0)\rangle = 175.78 \pm 1.52$ pN, while $\langle f_u(\Phi_c = 0.3)\rangle = 266.26 \pm 2.70$ pN. Thus, simulations with the AO potential led to a mean unfolding force that is roughly 50% greater than that in its absence. This disagrees sharply with the $\langle f_u(\Phi_c = 0.3)\rangle = 173.64 \pm 3.49$ pN resulting from our own simulations in the presence of an explicit crowding agent at $\Phi_c = 0.3$ and $r_f = 160 \times 10^3$ pN/s (Figure 4C). Indeed, the result also stands in marked contrast to the experimental results of Ping et al.[12] on octameric Ub, which saw a maximum increase in $\langle f_u\rangle$ of 21% (at $\Phi_c > 0.3$, $r_f = 4200$ pN/s, and with $\sigma_c \simeq 7.0$ nm) over the $\langle f_u\rangle = 166$ pN at $\Phi_c = 0$.[12]

There are a couple of origins to the discrepancy. First, the AO potential was derived to understand the equilibrium of colloidal spheres and plates in the presence of smaller-sized spherical crowding agents. Our experiments were of a nonequilibrium nature; therefore, it is somewhat unreasonable to expect such simulations to yield quantitatively accurate unfolding forces or dynamics. Second, as pointed out by Shaw and Thirumalai,[37] three-body terms are required to properly model depletion effects even in good solvents let alone in the poor solvent conditions of our simulations. To elaborate, let us consider the volume excluded to crowders by a Ub molecule, V_{ex}(Ub), to be the volume enclosed by a union of spheres of radii $S_i = (\sigma + \sigma_c)/2$. With an AO potential, the volume excluded to the spherical crowding agents is

$$V_E(\mathrm{Ub}) \simeq \sum_{i=1}^{N} V(S_i) - \sum_{j>i} V(S_i \cap S_j) \qquad (7)$$

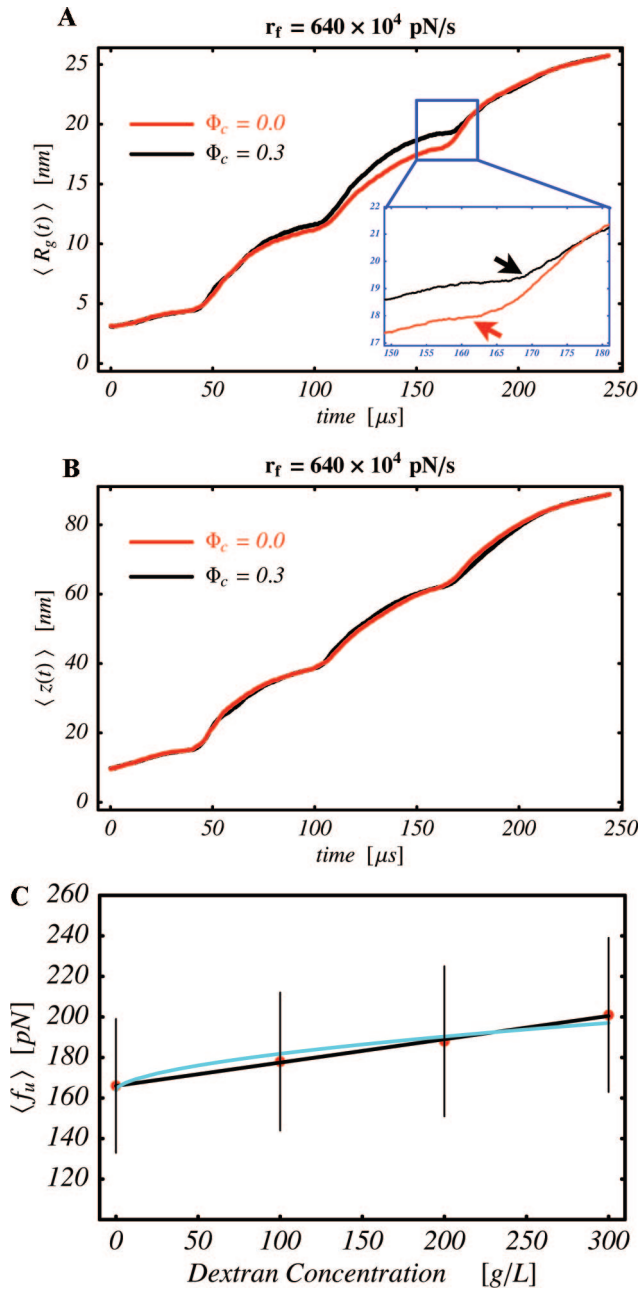

Figure 8. (A) $\langle R_g(t) \rangle$ versus time at $\Phi_c = 0$ (red) and 0.3 (black). Although the $\langle R_g \rangle$ increases more rapidly with time after the second rupture event at $\Phi_c = 0.3$ than that at $\Phi_c = 0$, the inset reveals that a larger R_g must be achieved to initiate the final rupture event in the presence of crowding particles with $\sigma_c = 6.4$ nm (see text for additional discussion). (B) $\langle z(t) \rangle$ versus time at $\Phi_c = 0$ (red) and 0.3 (black). $z(t)$ cannot discriminate between unfolding at the different volume fractions and hence is less suitable (than R_g) as a potential reaction coordinate. (C) The experimental results of Ping et al.[12] (red circles) for unfolding force, $\langle f_u \rangle$ as a function of dextran concentration, ρ. The black line is a fit assuming $\langle f_u \rangle \sim \rho$, and the blue is that assuming $\langle f_u \rangle \sim \rho^{5/9}$. Although both fits are consistent with the data, based on theoretical considerations (see eq 8), we prefer the blue fit (see text). (Standard deviations taken from Ping et al.[12])

where N is the number of residues in monomeric Ub (76), $V(S_i)$ is the volume of S_i and $V(S_i \cap S_j)$ is the volume associated with the overlap of S_i and S_j. Equation 7 neglects the overlap of three or more spheres. The importance of such overlaps, for soft spheres, increases as the crowders become much larger than the protein beads, and the neglect of such overlaps is the reason for the quantitative inaccuracy. As the size of the crowders increases (i.e., as the thickness of the depletion layer surrounding the protein beads increases), the surface enclosing Ub becomes more spherical, loses detail, and undoubtedly changes less in response to changes in the conformation of the molecule. Since depletion forces are proportional to the change in V_E(Ub) with respect to changes in Ub conformation, eq 7 overestimates the size of depletion forces in the presence of large crowders. Despite these limitations, the AO model, which is simple, can be used to provide qualitative predictions. Finally, we note that experiments typically use polyproteins to study force-induced unfolding (e.g., Ping et al.[12] used $(Ub)_8$ in their experiments). For polyproteins, the quantitative accuracy of the AO theory for unfolding in the presence of crowders of diameter $\sigma_c = 6.4$ nm is likely to increase because the volume excluded to the crowders will change significantly with changes in the conformation of the polyprotein.

$(Ub)_3$ at $\Phi_c = 0.0$ and 0.3. From arguments based on volume exclusion that lead to crowding-induced entropic stabilization of the folded structures, it follows that crowding effects should be more dramatic on polyUb than that on the monomer. In order to illustrate the effect of crowding on the stretching of $(Ub)_3$, we chose $\sigma_c = 6.4$ nm, which had negligible effect on $\langle f_u(\Phi_c) \rangle$ for the monomer. However, we found significant influence of the large crowding particles when $(Ub)_3$ was forced to unfold in their presence. The FEC (Figure 5) shows three peaks that corresponded to unfolding of the three domains when simulations were performed at crowder volume fractions of $\Phi_c = 0.0$ and 0.3 at $r_f = 640 \times 10^4$ pN/s. Figure 6 presents average unfolding forces as a function of the unfolding event number. Although the first two unfolding events were statistically indistinguishable at $\Phi_c = 0.0$ and 0.3, the final event occurred at much larger $\langle f_u \rangle$ in the presence of crowders than in their absence.

Order of Unfolding was Stochastic. $(Ub)_3$ has three chemically identical modules. In the pulling simulations, the N-terminus of module A was held fixed, while force was applied to the C-terminus of module C. Figure 7 illustrates the time dependence of contacts between secondary structure elements of modules A, B, and C. It is clear from Figure 7A that module C unfolded first, followed by module B, and finally by module A. On the other hand, the order of events in Figure 7B was A → C → B. The frequency with which the 3! = 6 possible permutations of these orders at $\Phi_c = 0$ and at $\Phi_c = 0.3$ were observed is presented in Table 1. It is clear that at both $\Phi_c = 0$ and 0.3, the most probable order of events was C → B → A. At $\Phi_c = 0$, this order was only marginally more probable than the order C → A → B, while at $\Phi_c = 0.3$, C → B → A became overwhelmingly more probable than any other unfolding order. In none of the simulations at $\Phi_c = 0$ or 0.3 did the rupture of module *C* occur as the final event.

Unfolding Within a Module Depended on the Proximity to the Point of Force Application. At $r_f = 640 \times 10^4$ pN/s, $(Ub)_3$ is fairly brittle, and the rupture of contacts within a module occurs nearly simultaneously. Nevertheless, by carefully examining time-dependent contact maps such as those illustrated in Figure 7, we were able to determine that (1) at both $\Phi_c = 0$ and 0.3 $\beta1/\beta5$ contacts were the first to rupture and (2) only for module C was this rupture event invariably followed by the loss of $\beta3/\beta5$ contacts. When other modules ruptured, loss of $\beta1/\beta5$ contacts was occasionally followed by loss of the $\beta1/\beta2$ strand pair contacts.

$(Ub)_3$ Must Achieve a Larger R_g to Rupture at $\Phi_c = 0.3$. Figure 8A illustrates the time dependence of $\langle R_g \rangle$ at $\Phi_c = 0$ and 0.3. Interestingly, the plot reveals that after the second

rupture event, the $\langle R_g(\Phi_c, t)\rangle$ increased more rapidly in the presence of crowders than in their absence. This is likely a reflection of the fact that at $\Phi_c = 0$ modules A and C were the first two modules to unfold in 44% of the trajectories, while at $\Phi_c = 0.3$, these two modules were the first to unfold in only 19% of trajectories. Thus, $\langle R_g(\Phi_c, t)\rangle$ increased more rapidly in the presence of crowders because the R_g of $(Ub)_3$ with two adjacent modules unfolded is larger than that with two unfolded but nonadjacent modules. Interestingly, these differences are masked in the time-dependent increase of the end-to-end distance (Figure 8B). Figure 8A also reveals that the horizontal inflection points marking the third unfolding event occur at different times at $\Phi_c = 0.3$ and in the absence of crowders. The difference between these two times was responsible for the difference in average unfolding forces of ≈14 pN illustrated in Figure 6. Thus, it is clear that despite the highly nonequilibrium nature of this pulling experiment, depletion effects were substantial, and it required a much greater force to reach f_u in the presence of these crowders than in their absence.

We predict that systematic experiments will reveal that polyUb molecules composed of larger numbers of modules will show greater increases in $\langle f_u(\Phi_c)\rangle$ relative to $\langle f_u(\Phi_c = 0)\rangle$ than polyUb molecules composed of fewer repeats. The size of these differences should increase with decreasing loading rate. Finally, it may even be possible to observe differences in the $\langle f_u\rangle$ as a function of the unfolding event number (as in Figure 6). The increase in $\langle f_u(\Phi_c)\rangle$, at a fixed Φ_c, for polyUb is likely to be even more significant for small crowding agents as shown in eq 8 (see below for further discussion).

Conclusions

General theory, based on the concept of depletion effects (see eqs 4 and 8), shows that crowding should enhance the stability of proteins and hence should result in higher forces to unfold proteins. However, predicting the precise values of $\langle f_u(\Phi_c)\rangle$ is difficult because of the interplay of a number of factors such as the size of the crowding agents and the number of amino acid residues in the protein. Despite the complexity, a few qualitative conclusions can be obtained based on the observation that when only excluded volume interactions are relevant then the protein or polyprotein would prefer to be localized in a region devoid of crowding particles.[40] The size of such a region is $D \approx \sigma_c(\pi/6\Phi_c)^{1/3}$. If $D \gg R_g$, then the crowding would have negligible effect on the unfolding forces. The condition $D \gg R_g$ can be realized by using large crowding particles at a fixed Φ_c. In the unfolded state, $R_g \approx 0.2N^{0.6}$ nm,[41] which for Ub leads to $R_g \approx$ 2.7 nm. Thus, $D/R_g = 0.4\sigma_c$. These considerations suggest that the crowder with $\sigma_c = 6.4$ nm would have negligible effect on the unfolding force, which is in accord with the simulations. On the other hand, $D/R_g \approx 0.4$ when $\sigma_c = 1$ nm, and hence, we expect that the smaller crowders would have measurable effect on the unfolding forces. Our simulations are in harmony with this prediction. We expect that for the smaller crowding agent, $\langle f_u(\Phi_c)\rangle$ would scale with Φ_c in a manner given by eq 8. In general, the appreciable effect of crowding on the unfolding forces can be observed only for large proteins or for polyproteins using relatively small crowding agents.

Although we have only carried out simulations for Ub and $(Ub)_3$ at one nonzero Φ_c, theoretical arguments can be used to predict the changes in $\langle f_u(\Phi_c)\rangle$ as Φ_c increases. The expected changes in the force required to unfold a protein can be obtained by using a generalization of the arguments of Cheung et al.[3] In the presence of crowding agents, the protein is localized in a region that is largely devoid of the crowding particles.[40] The most probable size of the region is $D \sim \sigma_c\Phi_c^{-1/3}$, where σ_c is the size of the crowding agent. If the structures in the DSE are treated as a polymer with no residual structure, then the increase in entropy of the DSE upon confinement is $\Delta S/k_B \sim (R_g/D)^{1/\nu}$, where R_g is the dimension of the unfolded state of the protein. If native-state stabilization is solely due to the entropic stabilization mechanism, we expect

$$\langle f_u(\Phi_c)\rangle \sim T\Delta S/L_c \sim \left(\frac{R_g}{\sigma_c}\right)^2 \Phi_c^{1/3\nu}\left(\frac{k_B T}{L_c}\right) \quad (8)$$

where $f_u(\Phi_c)$ is the critical force for unfolding the protein, L_c is the gain in contour length at the unfolding transition, and ν (≈0.588) relates R_g to the number of amino acids through the relation $R_g \sim a_D N^{\nu}$ (a_D varies between 2 and 4 Å). A few comments regarding eq 8 are in order. (1) The Φ_c dependence in eq 8 does not depend on the nature of the most probable region that is free of crowding particles. As long as the confining region, which approximately mimics the excluded volume effects of the macromolecule, is characterized by a single length D, we expect eq 8 to be valid. (2) The additional assumption used in eq 8 is that $N \gg 1$, and hence, there may be deviations due to finite size effects. (3) The equivalence between crowding and confinement breaks down at large Φ_c values. Consequently, we do not expect eq 8 to fit the experimental data at all values of Φ_c. (4) It follows from eq 8 that, for a given R_g, small crowding agents are more effective in stabilizing proteins than large ones. Thus, the prediction based on eq 8 is supported by our simulations. (5) From the variation of $\langle f_u(\Phi_c)\rangle$ with Φ_c, Ping et al.[12] suggest that $\langle f_u\rangle \sim \Phi_c$. However, the large errors in the measurements cannot rule out the theoretical prediction in eq 8. We have successfully fit their experimental results using eq 8 (Figure 8C). Additional quantitative experiments are required to validate the theoretical prediction.

It is difficult to map the concentrations in g/L used in the study of Ping et al.[12] to an effective volume fraction because of uncertainties in the molecular weight of dextran used in the study. Hence, a quantitative comparison between theory and experiments is challenging. A naive estimate may be obtained by using the values reported by Weiss et al.[42] Given that the dextran used in the study is thought to have an average molecular weight of 40 kDa and an estimated average hydrodynamic radius of 3.5 nm,[42] we find that $\rho = 300$ g/L corresponds to a volume fraction of $\Phi_c = 0.8$, which is very large. Nevertheless, Φ_c must be large when $\rho = 300$ g/L. Alternatively, we estimated $\sigma_c/2$ for dextran using $\sigma_c/2 \approx a_D N^{1/3}$, where N is the number of monomers in a 40 kDa dextran, which is 40/0.162 ≈ 147. If the monomer size is $a_D \approx 0.4-0.45$ nm, then we find $\Phi_c \approx 0.3-0.4$. If we assume that $\rho = 300$ g/L corresponds to $\Phi_c \simeq 0.4$ and that $\langle f_u(\Phi_c)\rangle \sim \Phi_c^{5/9}$ (eq 8), then at $\Phi_c = 0.3$, we would expect a nearly 18% increase in $\langle f_u\rangle$. Similarly, if $\rho = 300$ g/L corresponds to $\Phi_c \simeq 0.3$, then we would expect an increase in $\langle f_u\rangle$ of approximately 21%. In any case, we can say that at physiologically relevant volume fractions ($\Phi_c \in [0.1,0.3]$), the percent increase in $\langle f_u\rangle$ is likely to be ≤20%. Our simulations for $\sigma_c = 1.0$ nm predict an increase of 3−4%, which shows that a more detailed analysis is required to obtain an accurate value of σ_c for dextran before a quantitative comparison with experiments can be made. The larger increase seen in experiments may also be a reflection of the use of $(Ub)_8$ rather than a monomer.

Regardless of the crowder size, we find that the unfolding pathways are altered in the presence of crowding agents. It is

normally assumed that the rupture of secondary structure elements is irreversible if the applied force exceeds a threshold value. However, when unfolding experiments are carried out in the presence of crowding particles that effectively localize the protein in a smaller region than when $\Phi_c = 0$, reassociation between already ruptured secondary structures is facilitated as shown here. Thus, forced unfolding cannot be described using one-dimensional free-energy profiles with z_u as the reaction coordinate.[33]

We find that the average unfolding force for the final rupture event of the unfolding of $(Ub)_3$ occurred at much larger values in the presence of crowders than in their absence. With $\sigma_c = 6.4$ nm, which has practically no effect on the unfolding force of the monomer, and $\Phi_c = 0.3$, even with unfolding of two modules, the interactions between the stretched modules and protein are small ($D \approx 1.2\sigma_c$). Only upon unfolding of the third Ub do crowding effects become relevant, which leads to an increase in $\langle f_u(\Phi_c)\rangle$. Our results suggest that $\langle f_u(\Phi_c)\rangle/\langle f_u(0)\rangle$ should increase with the number of modules in the array and that it may be possible to detect differences in $\langle f_u\rangle$ which are conditional on the unfolding event number. We speculate that naturally occurring polyproteins that are subject to mechanical stress have evolved to take advantage of precisely such enhanced depletion effects.

Acknowledgment. This work was supported by a grant from the National Science Foundation (CHE 05-14056). D.L.P. is grateful for a Ruth L. Kirschstein Postdoctoral Fellowship from the National Institute of General Medical Sciences (F32GM077940). Computational time and resources for this work were kindly provided by the National Energy Research Scientific Computing (NERSC) Center.

References and Notes

(1) Zhou, H. X.; Rivas, G.; Minton, A. P. *Annu. Rev. Biophys.* **2008**, *37*, 375–397.
(2) Minton, A. P. *Biophys. J.* **2005**, *88*, 971–985.
(3) Cheung, M. S.; Klimov, D.; Thirumalai, D. *Proc. Natl. Acad. Sci. U.S.A.* **2005**, *102*, 4753–4758.
(4) Zhou, H. X. *Acc. Chem. Res.* **2004**, *37*, 123–130.
(5) Asakura, S.; Oosawa, F. *J. Chem. Phys.* **1954**, *22*, 1255–1256.
(6) Asakura, S.; Oosawa, F. *J. Polym. Sci.* **1958**, *33*, 183–192.
(7) Vrij, A. *Pure Appl. Chem.* **1976**, *48*, 471–483.
(8) Sasahara, K.; McPhie, P.; Minton, A. P. *J. Mol. Biol.* **2003**, *326*, 1227–1237.
(9) Stagg, L.; Zhang, S. Q.; Cheung, M. S.; Wittung-Stafshede, P. *Proc. Natl. Acad. Sci. U.S.A.* **2007**, *104*, 18976–18981.
(10) Homouz, D.; Perham, M.; Samiotakis, A.; Cheung, M. S.; Wittung-Stafshede, P. *Proc. Natl. Acad. Sci. U.S.A.* **2008**, *105*, 11754–11759.
(11) Cheung, M. S.; Thirumalai, D. *J. Phys. Chem. B* **2007**, *111*, 8250–8257.
(12) Ping, G.; Yang, G.; Yuan, J.-M. *Polymer* **2006**, *47*, 2564–2570.
(13) Yuan, J. M.; Chyan, C. L.; Zhou, H. X.; Chung, T. Y.; Haibo, J.; Ping, G.; Yang, G. *Protein Sci.* **2008**, *17*, 2156–2166.
(14) Fisher, T.; Marszalek, P.; Fernandez, J. *Nat. Struct. Biol.* **2000**, *7*, 719–724.
(15) Evans, E.; Ritchie, K. *Biophys. J.* **1997**, *72*, 1541–1555.
(16) Hyeon, C.; Thirumalai, D. *Biophys. J.* **2006**, *90*, 3410–3427.
(17) Hyeon, C.; Dima, R.; Thirumalai, D. *Structure* **2006**, *14*, 1633–1645.
(18) Hyeon, C.; Lorimer, G.; Thirumalai, D. *Proc. Natl. Acad. Sci. U.S.A.* **2006**, *103*, 18939–18944.
(19) Chen, J.; Dima, R.; Thirumalai, D. *J. Mol. Biol.* **2007**, *374*, 250–266.
(20) Hyeon, C.; Onuchic, J. *Proc. Natl. Acad. Sci. U.S.A.* **2007**, *104*, 17382–17387.
(21) Best, R. B.; Paci, E.; Hummer, G.; Dudko, O. K. *J. Phys. Chem. B* **2008**, *112*, 5968–5976.
(22) Karanicolas, J.; Brooks, C. L., III. *Protein Sci.* **2002**, *11*, 2351–2361.
(23) Li, M.; Kouza, M.; Hu, C. *Biophys. J.* **2007**, *92*, 547–561.
(24) Vijay-Kumar, S.; Bugg, C.; Cook, W. *J. Mol. Biol.* **1987**, *194*, 531–544.
(25) Kremer, K.; Grest, G. *J. Chem. Phys.* **1990**, *92*, 5057–5086.
(26) Pincus, D. L.; Cho, S. S.; Hyeon, C.; Thirumalai, D. Minimal models for proteins and RNA: From folding to function. In *Progress in Nucleic Acid Research and Molecular Biology*; Conn, P. M., Ed.; Elsevier Academic Press: San Diego, CA, arXiv:0808.3099v1 [q-bio.BM].
(27) Allen, M. P.; Tildesley, D. J. *Computer Simulation of Liquids*; Oxford University Press: New York, 1987.
(28) Ermak, D.; McCammon, J. *J. Chem. Phys.* **1978**, *69*, 1352–1360.
(29) Veitshans, T.; Klimov, D.; Thirumalai, D. *Folding Des.* **1996**, *2*, 1–22.
(30) Carrion-Vazquez, M.; Li, H.; Lu, H.; Marszalek, P.; Oberhauser, A.; Fernandez, J. *Nat. Struct. Biol.* **2003**, *10*, 738–743.
(31) Bockelmann, U.; Essevaz-Roulet, B.; Heslot, F. *Phys. Rev. E* **1998**, *58*, 2386–2394.
(32) Carrion-Vazquez, M.; Oberhauser, A.; Fowler, S.; Marszalek, P.; Broedel, S.; Clarke, J.; Fernandez, J. *Proc. Natl. Acad. Sci. U.S.A.* **1999**, *96*, 3694–3699.
(33) Hyeon, C.; Thirumalai, D. *J. Phys.: Condens. Matter* **2007**, *19*, 113101.
(34) Guo, Z.; Thirumalai, D. *Biopolymers* **1995**, *36*, 83–102.
(35) Mickler, M.; Dima, R.; Dietz, H.; Hyeon, C.; Thirumalai, D.; Rief, M. *Proc. Natl. Acad. Sci. U.S.A.* **2007**, *104*, 20268–20273.
(36) Peng, Q.; Li, H. *Proc. Natl. Acad. Sci. U.S.A.* **2008**, *105*, 1885–1890.
(37) Shaw, M. R.; Thirumalai, D. *Phys. Rev. A* **1991**, *44*, R4797–R4800.
(38) Verma, R.; Crocker, J.; Lubensky, T.; Yodh, A. *Phys. Rev. Lett.* **1998**, *81*, 4004–4007.
(39) Toan, N.; Marenduzzo, D.; Cook, P.; Micheletti, C. *Phys. Rev. Lett.* **2006**, *97*, 178301(4)
(40) Thirumalai, D. *Phys. Rev. A* **1988**, *37*, 269–276.
(41) Kohn, J. E.; Millet, I. S.; Jacob, J.; Zagrovic, B.; Dillon, T. M.; Cingel, N.; Dothager, R. S.; Seifert, S.; Thiyagarajan, P.; Sosnick, T. R.; Hasan, M. Z.; Pande, V. S.; Ruczinski, I.; Doniach, S.; Plaxco, K. W. *Proc. Natl. Acad. Sci. U.S.A.* **2005**, *101*, 14475–14475.
(42) Weiss, M.; Elsner, M.; Kartberg, F.; Nilsson, T. *Biophys. J.* **2004**, *87*, 3518–3524.
(43) Humphrey, W.; Dalke, A.; Schulten, K. *J. Mol. Graph.* **1996**, *14*, 33–38.

JP807755B